



HAL
open science

Exploring bron monitoring solutions in Pressurized Water Reactors for enhanced loss of coolant accidents mitigation

Nouhaila Tabti, Adrien Sari, Dominique Tromson

► **To cite this version:**

Nouhaila Tabti, Adrien Sari, Dominique Tromson. Exploring bron monitoring solutions in Pressurized Water Reactors for enhanced loss of coolant accidents mitigation. PHYSOR2024 - International Conference on Physics of Reactors, Apr 2024, San Francisco, United States. pp.Pages 336-345, 10.13182/PHYSOR24-43536 . cea-04924738

HAL Id: cea-04924738

<https://cea.hal.science/cea-04924738v1>

Submitted on 31 Jan 2025

HAL is a multi-disciplinary open access archive for the deposit and dissemination of scientific research documents, whether they are published or not. The documents may come from teaching and research institutions in France or abroad, or from public or private research centers.

L'archive ouverte pluridisciplinaire **HAL**, est destinée au dépôt et à la diffusion de documents scientifiques de niveau recherche, publiés ou non, émanant des établissements d'enseignement et de recherche français ou étrangers, des laboratoires publics ou privés.

Exploring Boron Monitoring Solutions in Pressurized Water Reactors for Enhanced Loss of Coolant Accidents Mitigation

Nouhaila Tabti*, Adrien Sari, Dominique Tromson

Université Paris-Saclay, CEA, List, F-91120 Palaiseau, France

ABSTRACT

Monitoring key parameters within Pressurized Water Reactors (PWRs) is crucial to mitigate the consequences of Loss of Coolant Accidents (LOCAs). This study aims to elucidate the prospective benefits and difficulties of deploying boron monitoring instrumentation in the Reactor Cooling System (RCS) for rapid and accurate LOCA assessment, encompassing break size and location. We comprehensively assess boron concentration evolution in PWR's coolant loops during 5-inch, 6-inch, and 7-inch cold leg breaks using the CATHARE-3 code for thermal-hydraulic simulations. Subsequently, we identify the optimal location for boron monitoring within the primary coolant loops to enhance the effectiveness and accuracy of boron concentration measurement during a LOCA. We also assess the performance of a preliminary design of a non-intrusive Boron Concentration Measuring System (BCMS) via Monte Carlo simulations using the MCNP6.2 code. Results derived from CATHARE-3 simulations indicate that placing the BCMS near the crossover (intermediate) leg offers advantages for both short-term and long-term LOCA scenarios. Differences in boron concentration between ruptured and intact loops identify compromised loop, while variations in boron concentration within the crossover leg correlate with break characteristics. Outcomes from MCNP6.2 calculations help to determine the ideal measuring configuration and expose the key challenges of incorporating boron instrumentation within the RCS, particularly regarding the impact of temperature on counting rates and resolving power.

Keywords: Pressurized Water Reactor (PWR), Boron Concentration Measuring System (BCMS), Loss of Coolant Accident (LOCA), CATHARE-3, MCNP6.2

1. INTRODUCTION

Boron, in the form of boric acid (H_3BO_3), is introduced into the primary coolant of Pressurized Water Reactors (PWRs) to finely modulate reactivity and power distribution within the core. This adjustment holds crucial importance in ensuring the reactor's stable and controlled operation. Boron-10 (^{10}B) exhibits a substantial neutron absorption cross section, of approximately 3845 barns when exposed to thermal neutrons with an energy of 25.3 meV. The deliberate addition of boron serves several indispensable functions during both normal reactor operation and operational transients. One of its primary roles involves offsetting fuel burnup and managing the dynamic behavior of xenon, a fission product with significant reactivity implications. Hence, the controlled introduction of boron plays a major role in maintaining the reactor's stability. Moreover, boron plays a critical role in preventing potential reactivity excursions within the core, which could lead to criticality-related issues. For example, in the event of a Loss of Coolant Accident (LOCA), a scenario fraught with challenges, highly borated water is rapidly injected into the primary system through the Emergency Core Cooling System (ECCS) in order to reestablish core cooling and accelerate shutdown processes. The intentional addition of boron in such circumstances prevents

* nouhaila.tabti@cea.fr

unintended criticality and ensures the safe and reliable operation of the reactor throughout its operational lifespan. Given the multifaceted and critical role that boron plays in reactor safety and performance, it is imperative to maintain continuous monitoring of boron concentration within the primary coolant.

In general, boron concentration is measured using various methods [1]. Among these, two widely adopted approaches are periodic chemical sampling and the use of the Boron Concentration Measuring System (BCMS), commonly known as "boron meter". Periodic chemical titration is recognized for its precision but comes with the drawback of generating radioactive waste and requiring substantial time for analysis. Conversely, BCMS offers real-time continuous monitoring of boron concentration but introduces a somewhat higher margin of measurement error compared to chemical titration. BCMS can be categorized based on its operational mode and level of intrusiveness. The first categorization distinguishes BCMS as either online (providing real-time measurements) or offline (conducting measurements at discrete intervals). Additionally, boron meters are categorized as either intrusive [2-5], requiring direct physical contact with the primary fluid, or non-intrusive [6-8], employing non-contact methods. These categorizations allow for tailored boron concentration monitoring in nuclear reactor applications, accommodating specific operational requirements and constraints.

In this study, we undertake an investigation into the prospective advantages associated with the monitoring of boron concentration in accidental circumstances, notably within the context of a Medium Break Loss of Coolant Accident (MBLOCA) scenario involving 5-inch, 6-inch, and 7-inch diameter break located within the cold leg of a nuclear reactor. Employing the CATHARE-3 computational code [9], our primary objective revolves around the identification of the most strategically optimal placement for the BCMS within the primary coolant circuit. Subsequently, we embark on an in-depth exploration of the design considerations surrounding a non-intrusive BCMS tailored for integration into the Reactor Cooling System (RCS). This process of performance exploration is conducted through Monte Carlo simulations, using the MCNP6.2 code [10].

2. MBLOCA-INDUCED BORON CONCENTRATION DYNAMICS

LOCAs are typically categorized into three primary classifications: Small Break Loss of Coolant Accident (SBLOCA), Medium Break Loss of Coolant Accident (MBLOCA), and Large Break Loss of Coolant Accident (LBLOCA). This classification scheme is grounded in both the examination of the distinct thermal-hydraulic implications on the reactor core attributed to each break size category and the facilitation of a more comprehensive evaluation and qualification of the ECCS. In the context of this investigation, the analytical scenarios under consideration involve break of 5-inch (12.7 cm), 6-inch (15.24 cm), and 7-inch (17.78 cm) diameters, situated within the cold leg of the pressurizer-containing loop. These specific break sizes fall within the purview of MBLOCAs.

2.1. Methodology and Steady State

In this paper, we investigate the dynamics of boron behavior during LOCAs, with a specific focus on MBLOCA. To conduct this analysis, we employ simulation techniques utilizing CATHARE-3, a system-scale code jointly developed by CEA, EDF, Framatome, and IRSN since 1979. CATHARE-3 is based on a modular "classical" two-phase six-equation flow model that incorporates rigorously a set of qualified closure laws.

The nodalization scheme of a typical three-loop PWR is presented in Figure 1. The core consists of 157 fuel assemblies, collectively generating a thermal output of approximately 2785 MW_{th}. Initially, we assume a uniformly distributed boron concentration across all three loops, set as 1000 ppm, while maintaining it at 2500 ppm in the ECCS (safety injection systems and accumulators).

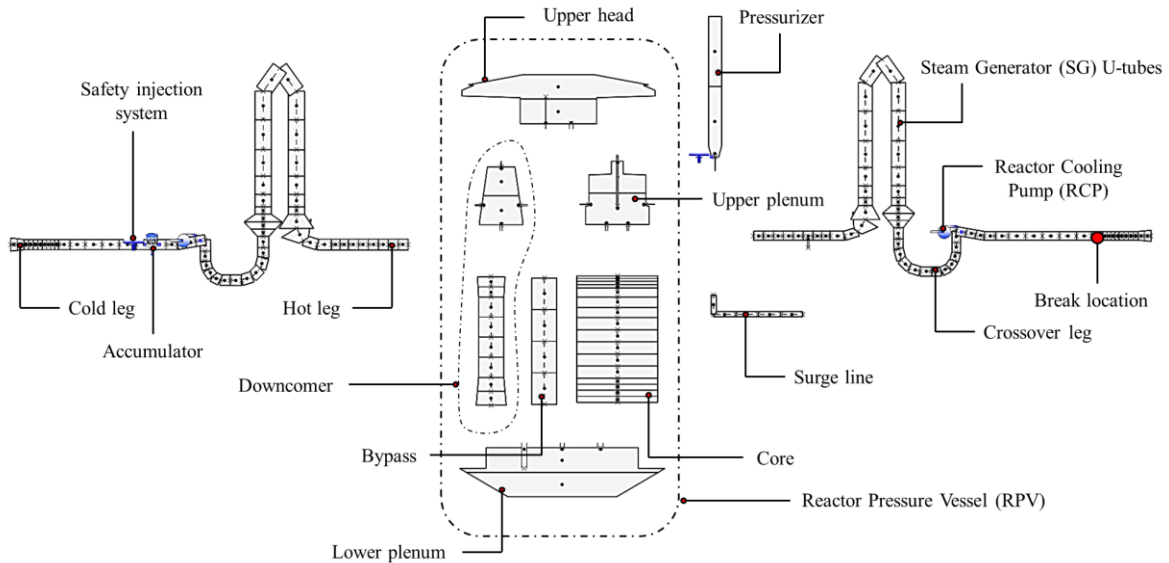


Figure 1. CATHARE-3 nodalization scheme of the primary system of a three-loop PWR.

2.2. MBLOCA Transients

In the context of a MBLOCA scenario in a PWR, we focus on a challenging case involving a primary coolant circuit break situated on the cold leg. This specific scenario represents one of the most critical conditions within the MBLOCA category in terms of its impact on core thermal-hydraulic behavior. It leads to the loss of ECCS flow, including safety injection and accumulator injection, in the affected loop. This, in turn, maximizes the flow loss at the break and delays the transition of the discharge at the break to a purely vapor phase, ultimately resulting in a high Peak Cladding Temperature (PCT). The sequence of events associated with the three simulated scenarios unfolds, as summarized in Table I and Figure 2, depicting the evolution of key characteristics in the primary system. Initially, a monophasic depressurization commences upon the opening of the break. This phase corresponds to the depressurization of the primary circuit (Figure 2a), effectively draining the pressurizer (Figure 2b). When the primary pressure drops to a low threshold of 12.95 MPa (SCRAM signal), control rods drop, and the nuclear power output is shutdown. For the purposes of this study, we assume that the Reactor Coolant Pumps (RCPs) are shutdown simultaneously with the SCRAM signal. Subsequently, upon reaching a much lower primary pressure threshold of 11.75 MPa, safety injection is actuated. After the complete shutdown of the RCPs, single-phase natural circulation, in the form of a thermosiphon, is established. The depressurization continues as the primary circuit's pressurizer continues to empty until saturation conditions are reached in the hottest areas of the circuit. The generation of vapor due to boiling in these zones significantly hampers the primary depressurization. Despite the continuous supply of liquid to the break, it proves inadequate to dissipate the residual core power, leading to a halt in depressurization while the primary circuit drainage persists. The subsequent phase witnesses the establishment of two-phase natural circulation with an increasing void fraction (where void fraction quantifies the proportion of gas phase within a defined volume, where 0 represents a completely liquid phase, and 1 signifies a pure gas phase) in the rising sections of the Steam Generators (SGs) tubes. However, when the continuous flow at the top of SGs tubes ceases, full phase separation takes place. Stratified drainage impacts both the rising and descending sections of SGs tubes, resulting in a liquid-vapor counter-current in the hot branches and rising sections, effectively marking the end of natural circulation and the onset of the reflux condenser mode. Throughout these phases, the break continues to lose liquid. The majority of residual core heat is removed by SGs, as long as the break mass flow remains single-phase liquid. During this phase, the energy balance is maintained, with the primary

system's mass loss continuing due to the ECCS's inability to compensate for the mass flow lost through the break. As the depressurization process progresses, stratified drainage occurs, leading to a drop in the level in the downward branches of the crossover legs. At this point, a water plug becomes trapped in the crossover leg of each loop. The transition of the break to a gas flow phase is contingent on a clear passage between the core and the break, which becomes possible after the expulsion of the water plugs within the broken primary loop. In the moments surrounding the expulsion of the water plugs, a decrease in the vessel's level (Figure 2c) may lead to a brief excursion of the fuel rod temperatures in the uncovered region, corresponding to the maximum PCT. This temperature should remain below 1204°C, in accordance with LOCA safety criteria, with the cladding's oxidation rate not exceeding 17%. Following the expulsion of the water plugs, a clear passage for vapor between the core and the break occurs, allowing the discharge at the break to transition to a pure vapor phase (Figure 2d). This transition leads to a significant shift in the primary system's energy balance. The persistent formation and evacuation of vapor enhance the extraction of decay heat from the core, resume primary depressurization, and cause the primary pressure to drop below the secondary pressure. Additionally, the transition of the break loss to a vapor phase positively affects the mass balance, as the loss of liquid mass becomes substantially lower. Simultaneously, depressurization contributes to an improved mass balance, since the reduction in pressure results in a lower break flow rate and an increase in flow rate injected by the ECCS. As the primary mass decreases at a slower rate, the ECCS injection rate may still be insufficient to compensate for the inventory deficit in the reactor vessel. However, when the accumulator injection pressure is reached at 4.2 MPa, it leads to a significant increase in the injection rate into the primary system. This results in an immediate rise in the total primary mass (Figure 2e), reflooding the core and returning temperatures to safe levels. The pressure drop comes to a halt when the energy balance shifts from surplus to equilibrium, with heat production and evacuation reaching a balanced state. Toward the end of the transient, there may be intermittent shifts in the break flow between liquid and vapor phases, resulting in mass flow oscillations (Figure 2d). Upon achieving final stabilization of primary pressure, the ECCS continue to function to ensure a continuous evacuation of residual heat. Note that the speed of the transient increases with the break size, as it directly influences the velocity of the draining and depressurization of the primary system (Table I).

Table I. Chronology of the main events of 5-inch, 6-inch and 7-inch MBLOCA.

Sequence	Time (s)		
	5-inch	6-inch	7-inch
Break opening	0	0	0
Reactor trip (SCRAM signal)	7	5	4
Safety injection actuation	10	7	5
Pressurizer empty	19	15	14
Start of safety injection pumps	41	37	36
No flow rate at the top of SG tubes for the broken loop	195	154	121
No flow rate at the top of SG tubes for the intact loop	202	167	129
Broken loop seals clearing	245	171	131
Core uncover	248	188	139
Intact loop seals clearing	270	193	140
Peak Clad Temperature (PCT)	190	210	227
Complete steam discharge at the break	312	211	161
Primary-secondary pressure reversal	339	229	166
Minimum primary side mass	523	369	265
Start of accumulators injection	524	369	265
End of accumulator discharge	1776	1457	1134
End of calculation	3000	3000	3000

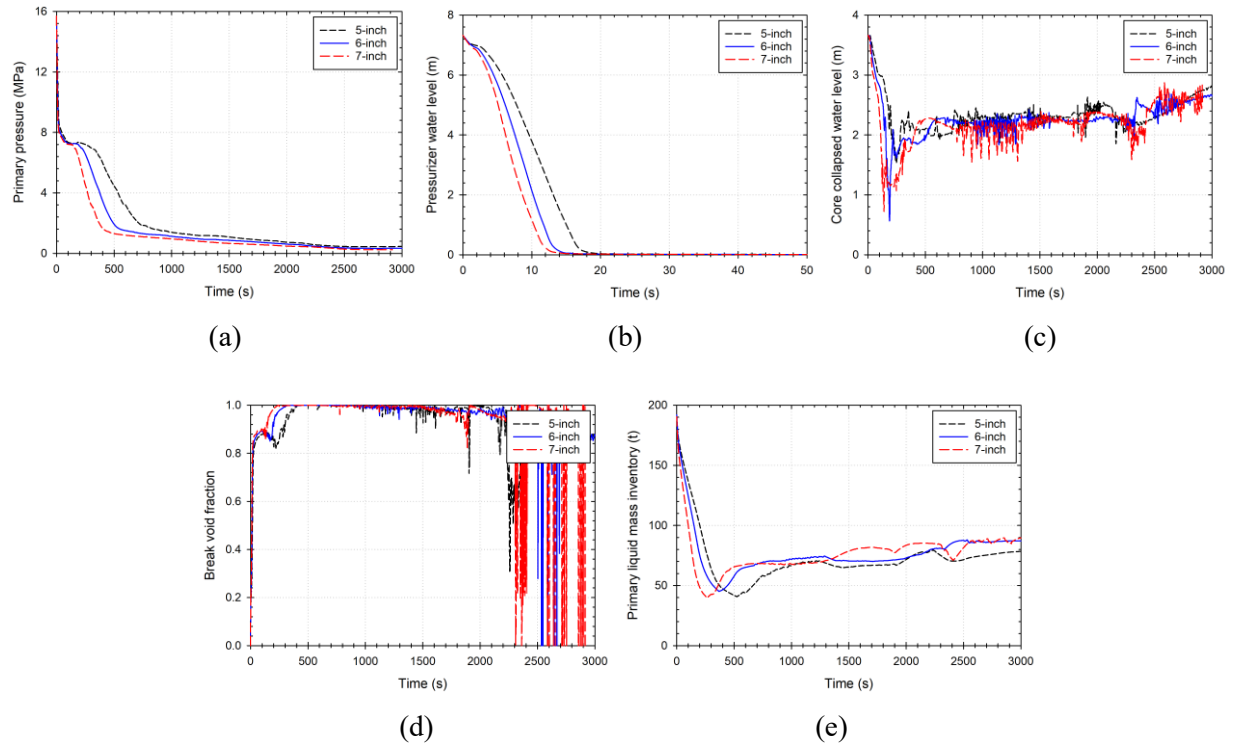


Figure 2. Temporal evolution of primary system main characteristics.

2.3. Optimal BCMS location

To determine the optimal placement of the BCMS within the primary system, particularly during unforeseen accidents such as a LOCA, it is imperative to evaluate the dynamic behavior of parameters that may affect BCMS performance. Among these parameters, void fraction stands out as a critical factor to consider. Notably, boron transport exclusively occurs within the liquid phase. Therefore, situating the BCMS in a region with a significant propensity to shift toward a dominant gas phase region would distort measurements, potentially rendering the boron meter ineffective in accidental scenarios. This underscores the necessity for a meticulous selection of the BCMS location within the primary system. To facilitate this selection process, we conducted comprehensive CATHARE-3 simulations to examine the void fraction evolution at specific mesh points within the system, encompassing the inlet, middle, and outlet locations of the hot, crossover, and cold legs, both in intact and broken loops. Figure 3 presents the outcomes of these simulations for the 6-inch MBLOCA scenario. Our observations indicate that, in general, the lowest void fractions throughout the transient occur within the crossover leg (Figures 3b and 3e). This observation aligns with expectations due to the unique U-shape and altimetry of the crossover leg, which facilitates fluid stratification in this region. As previously described, this stratification results in the formation of a water slug, hindering the passage of vapor generated by the core's decay heat. Leveraging this inherent disadvantage, we aim to provide operators with supplementary insights regarding break characteristics through the monitoring of boron concentration dynamics.

Therefore, we have determined the optimal position for the BCMS to be at the bottom of the lower section of the crossover leg. Building upon this selected location, we proceed to evaluate the evolution of boron concentration according to each simulated break size.

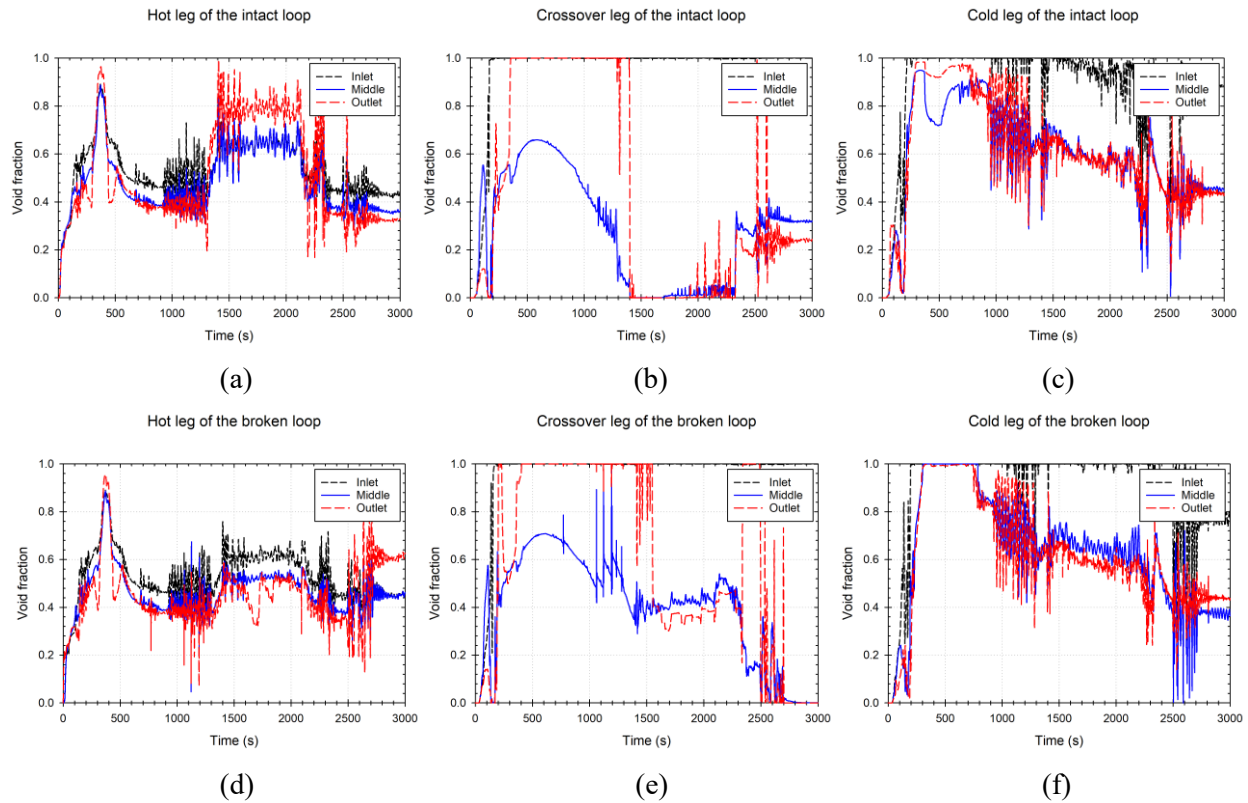


Figure 3. Void fraction evolution in hot, cold, and crossover legs during a 6-inch MBLOCA.

The simulation results, as depicted in Figure 4, reveal notable discrepancies in boron concentration levels between compromised and intact loops, facilitating the identification of the affected loop. It is essential to recognize that the dynamics of boron concentration are inherently intertwined with fluid dynamics and the velocity of circuit drainage. Furthermore, our findings affirm that the dynamics of boron concentration are intricately linked to the size of the break. Nonetheless, it is imperative to acknowledge that as the break size increases, the void fraction within the designated area for the boron meter similarly escalates as well. This phenomenon is evident in the graph representing void fraction evolution for a 7-inch break size, as seen in Figure 4f, ultimately resulting in a dominant gas phase within this region during some moments of the transient. This development compromises the precision of boron measurements, given the absence of liquid content to characterize. We, therefore, hypothesize that a specific break size demarcates the boundary between scenarios amenable to characterization and those classified as uncharacterized LOCAs, through the monitoring of boron dynamics. Moreover, the variation in void fraction underscores the necessity for BCMS calibration based on void fractions falling below a predetermined threshold. Additional investigations are warranted to elucidate this matter further. Looking ahead, we believe that BCMS, particularly in the context of long-term effects following LOCAs, could play a crucial role in preventing the transport of diluted slugs (red curves in Figures 4a and 4b) to the core. The development of nomograms and charts that correlate break characteristics with the evolution of boron concentration will empower operators to swiftly evaluate accidents, thereby enhancing safety protocols. In future applications, the dynamics of boron evolution could be seamlessly integrated into computational models, such as artificial neural networks or support vector machines [11], enabling rapid accident assessment while incorporating other parameters such as pressure and temperature.

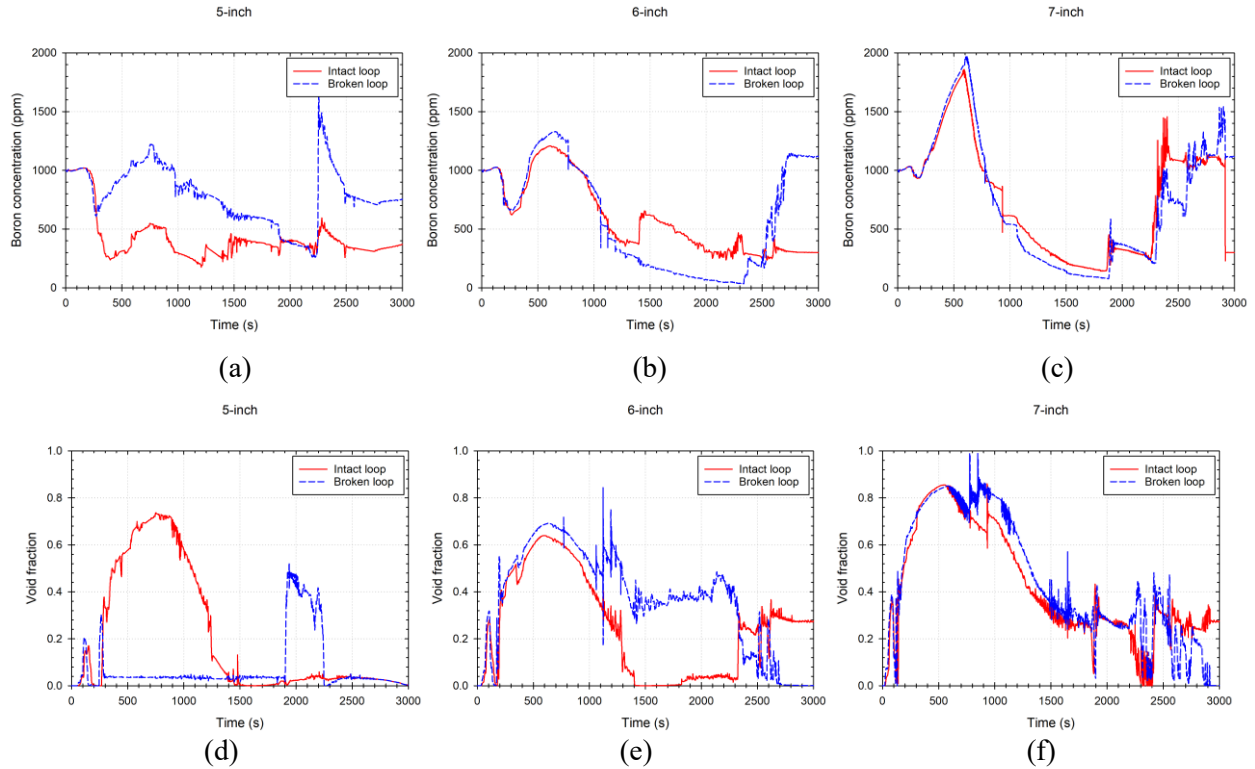


Figure 4. Boron concentration discrepancies and void fraction evolution: intact vs broken loops.

3. BCMS DESIGN CONSIDERATIONS AND PERFORMANCE EXPLORATION

The measurement principle of the BCMS is founded upon quantifying the attenuation of a neutron flux originating from a neutron source such as Am-Be. Neutrons undergo capture through the $^{10}\text{B}(n, \alpha)^7\text{Li}$ reaction after being effectively slowed down by an adequate neutron moderator, like light water, heavy water, graphite, or polyethylene. Subsequently, the remaining neutrons that reach the detector region provide a counting rate (in cps), corresponding to a certain boron concentration (in ppm). When siting a BCMS within the primary system, particularly in proximity to a primary large-size pipe, the significant volume of water contained within the pipe serves as a sufficient neutron moderator. The main objective of this investigation is to determine, using Monte Carlo simulation with the MCNP6.2 code, the optimal measuring configuration for a non-intrusive BCMS, positioned near the crossover leg as selected in section 2. Additionally, we aim to analyze the performance criteria [12] of the initial design to address the multifaceted challenges in quantifying boron concentration within the primary system. The insights gleaned from this preliminary study, which encompasses aspects like the BCMS's counting rate (CR), resolving power (relative difference in counting rate to a reference value; CR_{ref}), and neutron-to-thermal sensitivity (variation in counting rate due to boron concentration and temperature changes), constitute an essential foundation for guaranteeing the accuracy of boron concentration measurements. In normal operation and throughout operational transients, the mean temperature of the primary system may exhibit a noteworthy range, typically fluctuating between 20°C and 304°C . These fluctuations hinge on whether the reactor is actively generating power or is in a shutdown mode. In the context of accidental occurrences such as a LOCA, where the reactor undergoes a rapid SCRAM signal-induced shutdown, the primary system's temperature gradually diminishes until reaching an equilibrium at the final stages of the accident. Crucially, given the temperature-dependent nature of cross sections, it becomes imperative to assess its influence on the measuring performance of the BCMS.

To comprehensively assess the BCMS's overall performance, we conducted simulations considering a monoenergetic neutron source emitting neutrons of 2.5 MeV, and two CPNB48 boron-lined proportional counters manufactured by PHOTONIS. These counters exhibit a neutron sensitivity of 10 cps/nv. Utilizing two counters serves a dual purpose: enhancing data redundancy to strengthen overall system integrity and fortifying reliability to mitigate potential failures in the data acquisition and processing chain. The simulation setup involved positioning the neutron source and detectors in close proximity to a large-diameter pipe, reminiscent of the configuration in a three-loop PWR, as illustrated in Figure 5. The primary objective of this study is to optimize the placement of the neutron source and the detectors in relation to the pipe. In particular, we focused on the study of the influence of neutron counters angular positioning θ around the pipe, ranging between 10° and 350° , while covering a range of boron concentrations from 0 ppm to 5000 ppm. This assessment involved calculating the (n, α) reaction rate occurring within the boron deposition layer, located along the interior wall of the neutron counters, using the F4 tally to estimate the detection efficiency. The resulting CRs at different boron concentrations were crucial for determining the resolving power (R) of the BCMS, which indicates the system's ability to discern and resolve minute differences in boron concentration. The summarized results can be found in Figure 6.

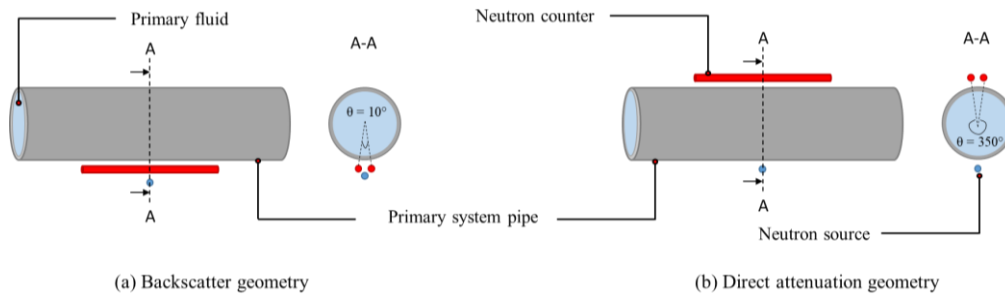


Figure 5. Schematic representation of direct attenuation and backscatter measuring configurations.

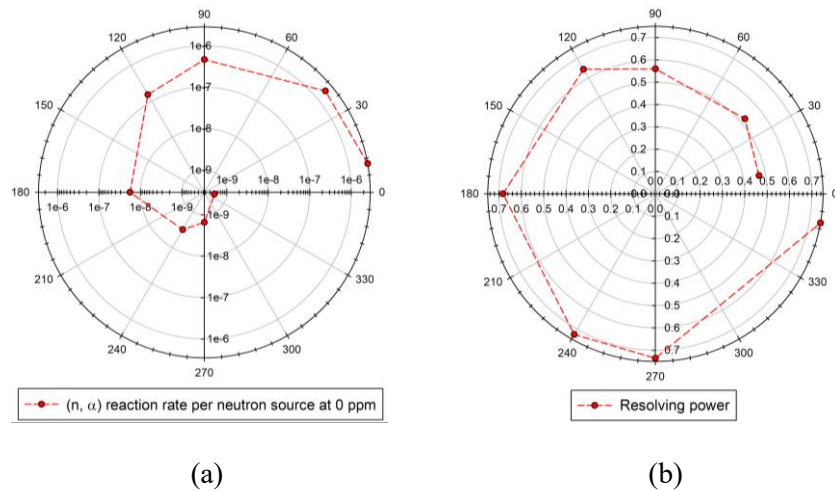


Figure 6. Impact of measuring configuration, MCNP6.2 simulation results.

The results revealed a discernible trend. Notably, as the detectors transitioned towards a direct attenuation configuration (Figure 5b), R substantially increased from 47% ($\theta = 10^\circ$) to 75% ($\theta = 350^\circ$), as shown in Figure 6b. However, a significant decrease in CR accompanies this transition, amounting to nearly three orders of magnitude (Figure 6a). This significant reduction, primarily attributed to the absorption of nearly all thermal neutrons by hydrogen within the primary fluid, poses a significant challenge to the statistical precision, warranting careful consideration.

Consequently, we select the backscatter-measuring configuration (Figure 5a), to balance CR and R effectively. Building upon this selected configuration, we embarked on an exploration of the influences of both fluid temperature (T_f) and detector temperature (T_{det}). Constrained by available cross sections and $S(\alpha,\beta)$ data [13], we undertook an evaluation of temperature's impact on measurement performance under two specific scenarios: one at ambient temperature (20°C) and the other at a considerably higher mean temperature of the primary system (277°C). The outcomes of our simulations, depicted in Figure 7, highlight a significant influence of elevated temperature levels on CR and R, with primary fluid temperature emerging as the dominant factor. A reduction in temperature by 257°C was observed to trigger an approximately 18% (at 0 ppm) decline in both CR and R (Figures 7a and 7b). Furthermore, upon examining neutron and thermal sensitivities, we discerned the prevailing dominance of thermal sensitivity (Figure 7c). This observation implies the minimalist design's sensitivity to temperature variations, warranting further investigation.

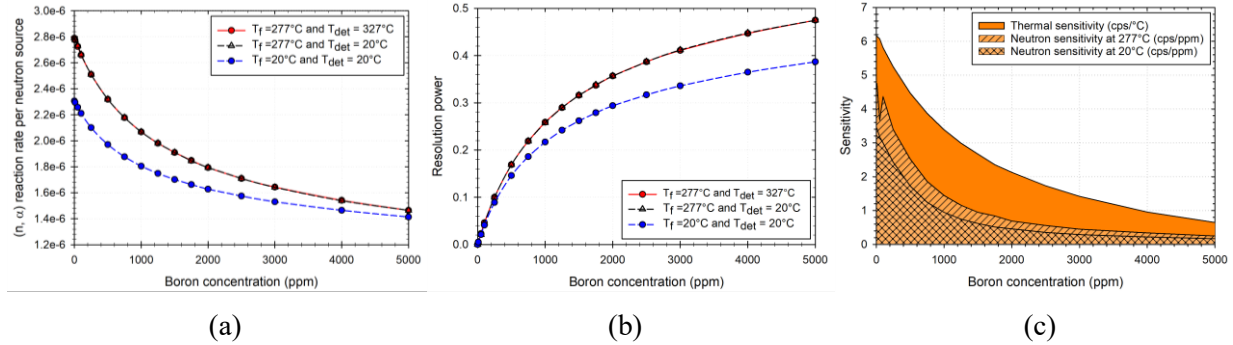


Figure 7. Impact of temperature, MCNP6.2 simulation results.

4. CONCLUSIONS AND OUTLOOK

This study has presented a comprehensive investigation of boron evolution during a LOCA. The primary focus of our analysis pertained to the evaluation of boron concentration dynamics within the primary coolant loops of a 900 MW_e PWR during a MBLOCA. We study various break sizes of 5-inch, 6-inch, and 7-inch, all situated in the cold leg of the primary loop containing the pressurizer. The overarching objective was to ascertain the most advantageous and optimal placement of the BCMS within the primary coolant system. It has become evident that the exploitation of data relating to boron concentration within the stratified fluid in the crossover leg can furnish operators with additional insights, thereby strengthening core safety and long-term plant integrity. Subsequently, we investigated the intricacies associated with the measurement of boron concentration within the primary coolant. Our findings have underscored two significant challenges. Firstly, the extensive volume of water within the primary loop legs led to a substantial reduction in counting rates due to the absorption of a significant proportion of neutrons following efficient moderation by hydrogen. Secondly, the broad spectrum of temperature fluctuations across the primary coolant engendered an unfavorable thermal-to-neutron sensitivity ratio. Furthermore, it is imperative not to disregard the harsh environmental factors within the containment building, including ambient radiation dose and gamma interference. Future endeavors in the optimization of advanced BCMS design will seek to mitigate these challenges. This proactive approach involves three main strategies. First, we will enhance neutron sensitivity by adopting higher-sensitivity neutron counters. Second, we aim at systematically exploring advanced neutron reflector materials to encompass the counters and improve measurement statistics. Third, we will introduce a gamma shield, potentially composed of materials such as lead, to envelop the detectors and minimize the occurrence of false positive counts. In addition to these measures, our future research direction will extend to the assessment of boron concentration transport and dynamics across a spectrum of LOCA scenarios, encompassing break sizes ranging from 1-inch to 14-inch.

This broader investigation seeks to comprehensively elucidate both the advantages and limitations of BCMS in diverse accident scenarios, thereby expanding the scope of BCMS applications across a more extensive range of LOCA scenarios.

ACKNOWLEDGMENTS

The authors are grateful to the CEA CATHARE team for their invaluable assistance and user support.

REFERENCES

- [1] R. N. Sah and P. H. Brown, "Boron Determination—A Review of Analytical Methods," *Microchemical Journal*, vol. 56, no. 3, pp. 285-304, 1997/07/01/ 1997, doi: 10.1006/mchj.1997.1428.
- [2] C. Kong, H. Lee, T. Tak, D. Lee, S. H. Kim, and S. Lyou, "Accuracy Improvement of Boron Meter Adopting New Fitting Function and Multi-Detector," (in English), *Nucl Eng Technol*, vol. 48, no. 6, pp. 1360-1367, Dec 2016, doi: 10.1016/j.net.2016.06.012.
- [3] S. H. Sung and H. R. Kim, "Development of accuracy enhancement system for boron meters using multisensitive detector for reactor safety," (in English), *Nucl Eng Technol*, vol. 52, no. 3, pp. 538-543, Mar 2020, doi: 10.1016/j.net.2019.08.004.
- [4] Y. Jo, C. Kong, J. Yu, D. Lee, and S. H. Kim, "High accuracy boronmeter design developed for light water reactors," *Ann Nucl Energy*, vol. 110, pp. 25-30, 2017.
- [5] S. H. Sung, U. J. Lee, J. S. Min, and H. R. Kim, "Experimental Setup for Boron Meter Accuracy Analysis in Nuclear Reactor Environment," (in English), *Materials in Environmental Engineering*, pp. 1201-1207, 2017, doi: 10.1515/9783110516623-118.
- [6] Framatome. "Boronline®, A new generation of boron meter. Technical Sheet No: A3022." (accessed April 15, 2022).
- [7] Mirion Technologies. "BM501™, Boronmeter. Technical Sheet No: 155780EN-F." <https://www.mirion.com/products/bm-501-boron-meter> (accessed November 23, 2021).
- [8] P. Pirat, "Boronline, a new generation of boron meter," in *2011 2nd International Conference on Advancements in Nuclear Instrumentation, Measurement Methods and their Applications*, 2011: IEEE, pp. 1-2.
- [9] P. Emonot, A. Souyri, J. L. Gandrille, and F. Barré, "CATHARE-3: A new system code for thermal-hydraulics in the context of the NEPTUNE project," *Nuclear Engineering and Design*, vol. 241, no. 11, pp. 4476-4481, 2011/11/01/ 2011, doi: 10.1016/j.nucengdes.2011.04.049.
- [10] C. J. Werner *et al.*, "'MCNP6.2 Release Notes", Los Alamos National Laboratory, report LA-UR-18-20808 " 2018.
- [11] T.-H. Lin, C. Chen, S.-C. Wu, T.-C. Wang, and Y.-M. Ferng, "Localization and size estimation for breaks in nuclear power plants," *Nucl Eng Technol*, vol. 54, no. 1, pp. 193-206, 2022/01/01/ 2022, doi: 10.1016/j.net.2021.07.007.
- [12] N. Tabti, A. Sari, and D. Tromson, "Towards the enhancement of nuclear reactor safety: physical phenomena involved in the measurement accuracy of boron concentration online monitoring systems," *IEEE Transactions on Nuclear Science*, 2023, doi: 10.1109/TNS.2024.3351481.
- [13] D. A. Brown *et al.*, "ENDF/B-VIII. 0: the 8th major release of the nuclear reaction data library with CIELO-project cross sections, new standards and thermal scattering data," *Nuclear Data Sheets*, vol. 148, pp. 1-142, 2018.